6th European Conference on Computational Mechanics (ECCM 6)
7th European Conference on Computational Fluid Dynamics (ECFD 7)
1115 June 2018, Glasgow, UK

FLUID-STRUCTURE AND ELECTRIC INTERACTION ANALYSIS OF PIEZOELECTRIC FLAP IN A CHANNEL USING A STRONGLY COUPLED FEM SCHEME

Prakasha Chigahalli Ramegowda[1], **Daisuke Ishihara**[1], **Rei Takata**[1], **Tomoya Niho**[1], **Tomoyoshi Horie**[1]

[1]Department of Mechanical Information Science and Technology,
Kyushu Institute of Technology, 680-4 Kawazu, Iizuka, Fukuoka, Japan

Key words: Fluid-Structure Interaction (FSI), Electric and Fluid-Structure Interaction (EFSI), Micro-Electro-Mechanical System (MEMS), bimorph actuator, flexible flap in a channel

Abstract. Electric and Fluid-Structure interaction (EFSI) is a complex coupled multi-physics phenomenon appears in microelectromechanical system (MEMS) when these microdevices are operated in a fluid media. In this study, the EFSI phenomena refer to a combination of electromechanical (electric-structure interaction) coupling and fluid-structure interaction coupling. Both the electromechanical coupling and the fluid-structure interaction can be simulated in a monolithic way or in a partitioned iteration way. In the proposed method the electromechanical coupling is simulated in a partitioned iterative way with separate solvers for the electrical and mechanical equations using block Gauss-Seidel (BGS) iteration method, while the fluid-structure interaction is simulated in a monolithic way by solving the fluid and structure equations simultaneously using a projection method. The proposed algorithm combines these two methods to analyze the strongly coupled EFSI in MEMS. The proposed method is applied to a flexible flap made of piezoelectric bimorph actuator in a converging channel. The EFSI analysis results show a good agreement with FSI results when a very low input bias voltage is applied to the actuator.

1 INTRODUCTION

Mimicking insect flapping flight for MEMS-based MAVs is actively pursued in the recent years using finite element coupled algorithms [1]. The flexible wing of an insect-like MEMS-based MAVs surrounded by air is actuated by the piezoelectric actuator. It is imperative to analyze the interaction between the fluid-structure and electric fields. Therefore, we propose the flexible piezoelectric bimorph flap in a channel to illustrate this novel interaction. Note that the original flap in a channel has been described in [2], which is known as one of the typical problems to test the convergence properties of computational fluid-structure interaction.

In this study, we present a numerical study of EFSI using a strongly coupled finite element algorithm applied to the benchmark problem. Here, the flexible piezoelectric bimorph flap is made of PVDF material and it is actuated by means of AC voltage as defined in [3, 4] along with the inlet fluid velocity boundary condition in a converging channel as defined in [2]. We

employed a projection method for the monolithic coupling of incompressible fluid and a structure [5]. The electro-mechanical coupling in a bimorph actuator is solved by employing block Gauss-Seidel scheme [3]. They are combined via the novel forces, moments and displacement translations [4] following the field decomposition approach [10]. The results obtained from the proposed method are very close to those in [2, 5] when a very low input voltage is applied to the actuator as the fundamental validation.

2 Formulation of Electric and Fluid-Structure Interaction (EFSI)

2.1 Formulation of electromechanical coupling in piezoelectric effect

The finite element equations of linear piezoelectricity are given as [3]

$$\mathbf{M_{uu}}\ddot{\mathbf{u}} + \mathbf{K}_{\mathrm{uu}}\mathbf{u} + \mathbf{K}_{\mathrm{u}\phi}\boldsymbol{\phi} = \mathbf{F}, \tag{1}$$

$$\mathbf{K}_{\mathrm{u}\phi}^{\mathrm{T}}\mathbf{u} + \mathbf{K}_{\phi\phi}\boldsymbol{\phi} = \mathbf{q}, \tag{2}$$

where $\mathbf{M_{uu}}$ is the mass matrix, $\mathbf{K}_{\mathrm{uu}}$ is the mechanical stiffness matrix of the structure, $\mathbf{K}_{\mathrm{u}\phi}$ is the piezoelectric stiffness matrix, $\mathbf{K}_{\phi\phi}$ is the dielectric stiffness matrix, $\mathbf{u}$ is the mechanical displacements, $\mathbf{F}$ is the external mechanical forces, ϕ is the electric potentials, $\mathbf{q}$ is the external surface density charges of the piezoelectric actuator, and a superscript T indicates the transpose of a matrix.

The direct piezoelectric effect is analyzed using solid elements as [4]

$${}^{t+\Delta t}\mathbf{K}_{\phi\phi}^{(i)}\ {}^{t+\Delta t}\boldsymbol{\phi}_{\mathrm{solid}}^{(i)} = {}^{t+\Delta t}\mathbf{q} - {}^{t+\Delta t}\mathbf{u}_{\mathrm{solid}}^{(i-1)}. \tag{3}$$

where i indicates the current each block Gauss-Seidel (BGS) iteration and the displacements ${}^{t+\Delta t}\mathbf{u}_{\mathrm{solid}}^{(i-1)}$ in the solid elements are obtained using the displacement transformation as

$$\mathbf{u}_{\mathrm{solid}} = {}^{\mathrm{u}}\mathbf{T}\mathbf{u}_{\mathrm{shell}}, \tag{4}$$

where ${}^{\mathrm{u}}\mathbf{T}$ is the displacement transformation matrix, and the left-hand superscript u stand for "displacement". Substituting the Eq. (4) into Eq. (3) yields the nonlinear direct piezoelectric equation to solve the electric potential in the solid elements as

$${}^{t+\Delta t}\mathbf{K}_{\phi\phi}^{(i)}\ {}^{t+\Delta t}\boldsymbol{\phi}_{\mathrm{solid}}^{(i)} = {}^{t+\Delta t}\mathbf{q} - {}^{\mathrm{u}}\mathbf{T}\ {}^{t+\Delta t}\mathbf{u}_{\mathrm{shell}}^{(i-1)}. \tag{5}$$

Solving the Eq. (5) yields the electric forces in the solid elements as

$${}^{\mathrm{e}}\mathbf{F}_{\mathrm{solid}} = \mathbf{K}_{\mathrm{u}\phi}\boldsymbol{\phi}. \tag{6}$$

As depicted in the Fig. 1 the induced electrical forces and moment of electric forces in solid elements are transformed onto shell elements to evaluate the inverse piezoelectric effect as

$$\mathbf{F}_{\mathrm{shell}} = {}^{\mathrm{e}}\mathbf{T}\ {}^{\mathrm{e}}\mathbf{F}_{\mathrm{solid}}, \tag{7}$$

where $\mathbf{F}_{\mathrm{shell}}$ is the equivalent force vector at the shell elements, ${}^{\mathrm{e}}\mathbf{F}_{\mathrm{solid}}$ is the induced electric force vector in the solid elements, ${}^{\mathrm{e}}\mathbf{T}$ is the transformation matrix, and the left-hand superscript e stand for "electric."

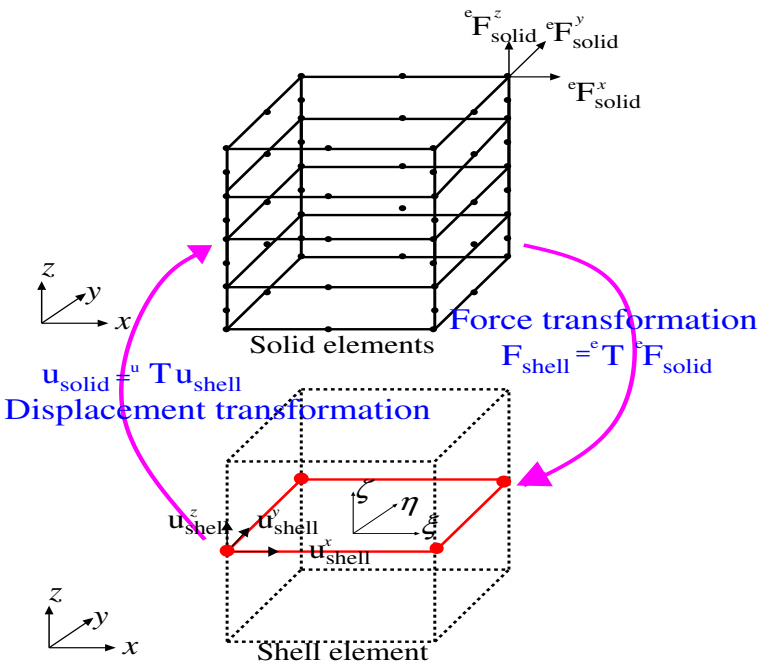

Figure 1: Electric force and displacement transformation between the solid and the shell elements

.

The structural equation is solved using shell element in the Total Lagrangian formulation with the full Newton–Raphson (N–R) iteration is [4]

$$ {}^{t+\Delta t}_{0}\hat{\mathbf{K}}^{(k-1),(i)}_{\mathrm{uu}}\ \boldsymbol{\Delta}\mathbf{u}^{(k),(i)} = \Delta\mathbf{R} - {}^{t+\Delta t}\mathbf{K}^{(i)}_{\mathrm{u}\phi}\ {}^{t+\Delta t}\boldsymbol{\phi}^{(k)}, \tag{8} $$

where k indicates the full Newton–Raphson iteration, $\Delta\mathbf{R}$ is the out-of-balance force vector, and $\boldsymbol{\Delta}\mathbf{u}^{(k),(i)}$ is the incremental displacement at BGS and Newton–Raphson (N–R) iteration in a time step. Substituting the force transformation equation in Eq. (7) to Eq. (8) yields

$$ {}^{t+\Delta t}_{0}\hat{\mathbf{K}}^{(k-1),(i)}_{\mathrm{uu}}\boldsymbol{\Delta}\mathbf{u}^{(k),(i)}_{\mathrm{shell}} = \Delta\mathbf{R} - {}^{\mathrm{e}}\mathbf{T}\ {}^{t+\Delta t}\mathbf{F}^{(k-1)(i)}_{\mathrm{solid}}, \tag{9} $$

The displacement approximation in the shell elements is corrected at every BGS and N–R iterations as

$$ {}^{t+\Delta t}\mathbf{u}^{(k),(i)}_{\mathrm{shell}} = {}^{t+\Delta t}\mathbf{u}^{(k-1),(i)}_{\mathrm{shell}} + \boldsymbol{\Delta}\mathbf{u}^{(k),(i)}_{\mathrm{shell}}. \tag{10} $$

2.2 Formulation of fluid–structure interaction

The equilibrium equation for the incompressible Navier-Stokes equations and the elastic body are considered to describe the motion of the fluid and the elastic body, respectively. The finite element formulation of the fluid-structure interaction (FSI) is based on the projection method. A projection method using the algebraic splitting was proposed by Ishihara and Horie

[5] which is based on the monolithic method where the discretized equation systems for the incompressible viscous fluid and the structure are solved simultaneously.

The monolithic equation system for the FSI can be obtained as [6]

$$ {}_{\mathrm{L}}\mathbf{M}\mathbf{a} + \mathbf{C}\mathbf{v} + \mathbf{N} + \mathbf{q}(\mathbf{u}) - \mathbf{G}\mathbf{p} = \mathbf{g}, \tag{11} $$

$$ {}_{\tau}\mathbf{G}\mathbf{v} = 0, \tag{12} $$

where ${}_{\mathrm{L}}\mathbf{M}$, $\mathbf{C}$, and $\mathbf{G}$ are the lumped mass, diffusive, and divergence operator matrices, $\mathbf{N}$, $\mathbf{q}$, $\mathbf{g}$, $\mathbf{a}$, $\mathbf{v}$, $\mathbf{u}$, and $\mathbf{p}$, are the convective term, elastic internal force, external force, acceleration, velocity, displacement, and pressure vectors, respectively. The Eqs. (11) and (12) are linearized using the increments of the acceleration $\Delta\mathbf{a}$, velocity $\Delta\mathbf{v}$, displacement $\Delta\mathbf{u}$, and pressure $\Delta\mathbf{p}$ to obtain the following simultaneous equation system:

$$ {}^{*}\mathbf{M}\Delta\mathbf{a} - \mathbf{G}\Delta\mathbf{p} = \Delta\mathbf{g}, \tag{13} $$

$$ \gamma\Delta t_{\tau}\mathbf{G}\Delta\mathbf{a} + \mathbf{G}_{\varepsilon}\Delta\mathbf{p} = \Delta\mathbf{h}, \tag{14} $$

where $\Delta\mathbf{g}$ and $\Delta\mathbf{h}$ are the residual vectors of Eqs. (11) and (12), respectively. $\mathbf{G}_{\varepsilon}$ comes from the pressure stabilization term of the PSPG method [8], and ${}^{*}\mathbf{M}$ is the generalized mass matrix, which is defined as

$$ {}^{*}\mathbf{M} = {}_{\mathrm{L}}\mathbf{M} + \gamma\Delta t\mathbf{C} + \beta\Delta t^{2}\mathbf{K}, \tag{15} $$

where $\mathbf{K}$ is defined using the tangential matrix of the structure [5]. The predictor-multi corrector algorithm (PMA) [7] based on Newmark's β method is used for the time integration of FSI equations. The projection method proposed is used to split the fluid-structure interaction into the structure-fluid velocity and then the pressure field [5]. It is briefly described as follows: From the equilibrium Eq. (11) the state variables are predicted as the intermediate state variables for the known pressure and it is linearized as

$$ {}^{*}\mathbf{M}\Delta\hat{\mathbf{a}} = \Delta\mathbf{g}. \tag{16} $$

where $\Delta\hat{\mathbf{a}}$ is the increment of the intermediate acceleration $\hat{\mathbf{a}}$. Subtracting both sides of Eq. (16) and Eq. (13) and after suitable arrangement we obtain

$$ \gamma\Delta t\mathbf{G}\Delta\mathbf{p} = {}^{*}\mathbf{M}(\mathbf{v} - \hat{\mathbf{v}}), \tag{17} $$

where $\hat{\mathbf{v}}$ is the intermediate velocity. Using the intermediate velocity $\hat{\mathbf{v}}$, the pressure increment $\Delta\mathbf{p}$ is obtained solving the pressure Poisson equation (PPE) as

$$ \gamma\Delta t_{\tau}\mathbf{G}_{\mathrm{L}}\mathbf{M}^{-1}\mathbf{G}\Delta\mathbf{p} = -{}_{\tau}\mathbf{G}\hat{\mathrm{v}}, \tag{18} $$

2.3 Electric-Structure-Fluid Interaction analysis

The strongly coupled electric-structure interaction given in Eq. (5) and Eq. (9) using BGS partitioned iteration and strongly coupled monolithic FSI equations using projection method given in Eqs. (13), (14), (16) and (18) are combined to analyze the electric-structure-fluid Interaction using a transformation scheme as show in Fig. 2. The proposed EFSI method is summarized as follows:

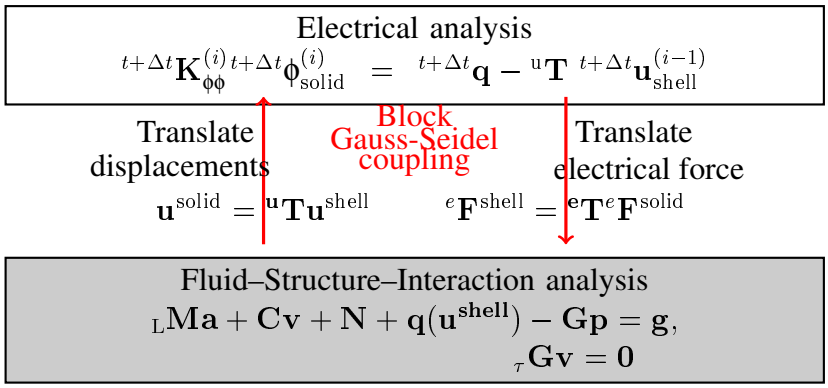

Figure 2: Symbolical presentation of Electric-Structure-fluid interaction algorithm

- The electric potential is obtained solving Eq. (5).
- The induced electrical forces are transformed onto shell structure as externally applied forces using Eq. (7).
- The increment of the intermediate acceleration $\Delta\hat{\mathbf{a}}$ is obtained by solving Eq. (16) and then the intermediate velocity is obtained.
- The pressure increment $\Delta\mathbf{p}$ is obtained by solving pressure Poisson equation (PPE) in Eq. (18).
- The acceleration increment $\Delta\mathbf{a}$ is obtained by solving the equilibrium Eq. (13).
- The current displacement ${}^{t+\Delta t}\mathbf{u}_{\text{shell}}^{(k),(i)}$ is obtained from Eq. (10).
- The resultant displacements in the shell element is transformed to the solid elements using Eq. (4).

3 Numerical example

3.1 problem setup

The numerical problem shown in Fig. 3(a) was first proposed by Neumann *et al*. in [2] in order to demonstrate the convergence properties, computational efficiencies and mesh sensitivity analysis of the FSI algorithms. In [5] the same problem was analyzed to discuss the convergence properties, computational efficiency and stability performances of projection method. The results obtained in [5] shows a good agreement with the benchmark results in [2]. In [2, 5], the flexible solid beam is made of a rubber with density $\rho^s = 1500\ \text{kg/m}^3$, Young's modulus $E^s = 2.3\text{MPa}$, and a Poisson's ratio $\nu^s = 0.45$. Since rubber is a non–piezoelectric material, in this study, a piezoelectric bimorph actuator made of Polyvinylidene fluoride (PVDF) with density $\rho^s = 1800\ \text{kg/m}^3$, Young's modulus $E^s = 2.0\text{GPa}$, Poisson's ratio $\nu^s = 0.29$, piezoelectric stress constant $e_{31} = 0.046\ \text{C/m}^2$,and a relative permitivity of $\epsilon_r = 12$ is used instead of rubber as shown in Fig. 3(b). The fluid is a silicon oil. The mass density and the viscosity of silicon

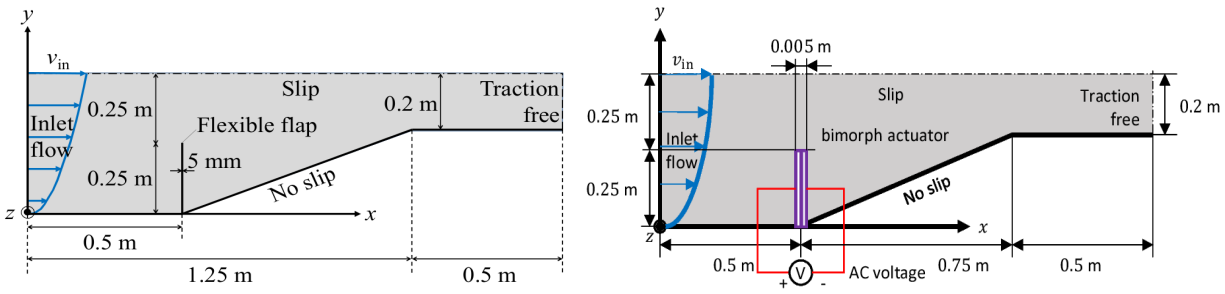

(a) FSI: A flexible flap in a fluid channel [2, 5] (b) EFSI: A piezoelectric bimorph actuator in a fluid channel

Figure 3: A piezoelectric bimorph actuator in the converging channel

oil used in the analysis are $\rho^f = 956\ \mathrm{kg/m^3}$ and $\mu^f = 0.145\mathrm{kg/(m.s)}$. As shown in the Fig. 4, the inflow velocity of the fluid has a parabolic shape. The fluid velocity at the top v_{in} varies as $V_{in}(1 - \cos 2\pi f t)$ ($V_{in} = 0.06067\mathrm{m/s}$ and $f = 0.05\mathrm{Hz}$) until 10 sec and V_{in} after 10 sec. The bimorph actuator is subjected to an applied AC voltage $V_\phi = V_{\phi_0} \sin \omega_\phi t$, as shown in Fig. 3(b). The dimensions of the fluid channel and the piezoelectric cantilever beam is depicted in Fig. 4.

Results computed with the [2, 5] show the maximum velocity at time $t = 10\mathrm{s}$ and after maximum velocity is reached, the flap starts retracting until its steady-state position. In this study, a harmonic oscillation is expected about the reference solutions when an AC input voltage source is applied to the reference setup in [5]. The vibration about the exact solution appears because of the inverse piezoelectric effect.

3.2 Analysis setup

The fluid domain of the channel is modeled using P1P1 elements [8] (12,012 nodes and 33,600 elements) shown in Fig. 4(a), the structural mesh of the piezoelectric cantilever beam is modeled using a mixed interpolation of tensorial components (MITC) [9](42 nodes and 20 elements) shown in Fig. 4(b) and the electrical field is analyzed using 3D solid elements (20 node hexahedron element) shown in Fig. 4(c) consists of 683 nodes and 80 elements. Both fluid and structural meshes have single division along the z direction as shown in Figs. 4(a) and 4(b) therefore the FSI setup is a two-dimensional problem, while the electrical setup is a three dimensional as shown in Fig. 4(c). There is a single division of the structural mesh in the z direction as shown in Fig. 4(b). The time step size used in the analysis is equal to $\Delta t = 0.005\mathrm{s}$ The piezoelectric bimorph actuator is connected in series type [3].

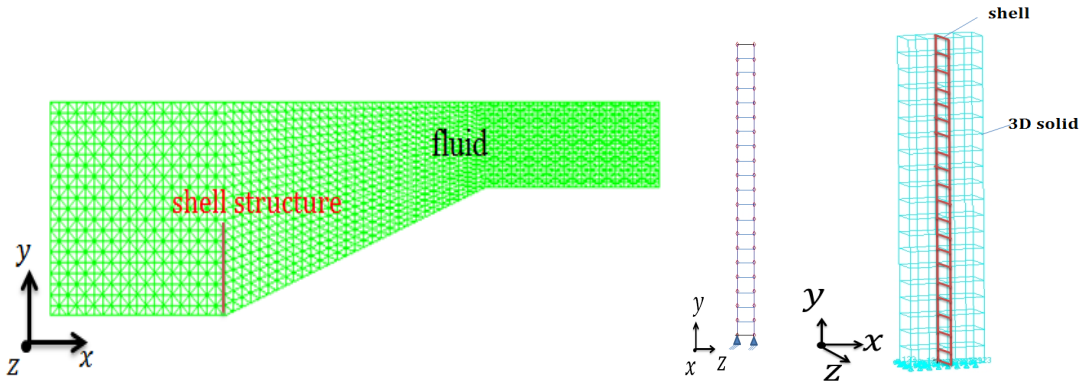

(a) (b) (c)

Figure 4: The finite element meshes: (a) Fluid analysis using P1P1 elements, (b)Structure analysis using Shell elements, (c) Electrical analysis using 3D solid elements

3.3 Results and discussions

The frequency response of a piezoelectric actuator is a primary design consideration in MEMS application. Therefore, in this study, a piezoelectric bimorph actuator in a converging fluid channel is actuated at various input voltage frequency ω_ϕ along with the imposed fluid velocity boundary conditions using the proposed EFSI method. The theoretical solution for the resonance frequency of the bimorph cantilever beam immersed in fluids is given as [11]

$$\omega_{(n)}^{fld} = \omega_{(n)}^{vac}\left[1 + \frac{\pi\rho^f b}{4\rho^s h}\Gamma_f(k)\right]^{-1/2}, \tag{19}$$

where ρ^f and ρ^s are the density of the fluid and the structure, respectively, b, and h are the width and the thickness of the structure, $\Gamma_f(k)$ is the hydrodynamic function, k is the normalized mode numbers and $\omega_{(n)}^{vac}$ is the resonant frequency in vacuum. The resonance frequency of the cantilever in vacuum is given as [11]

$$\omega_{(n)}^{vac} = \frac{\alpha_n^2}{L^2}\sqrt{\frac{E^s I}{m^s}}, \tag{20}$$

where $\alpha_1 = 1.875$ corresponds to the fundamental flexural mode, I is cross-sectional area moment of inertia and m^s is the mass per unit of length. The transverse resonant frequency of the bimorph actuator in vacuum [11] for the bimorph actuator dimensions $L = 0.25\text{m}$, $b = 0.02\text{m}$ and $h = 0.005\text{m}$ is $\omega_{(1)}^{vac} = 85.58\ \text{rad/s}$. Similarly, the theoretical transverse resonant frequency of the bimorph actuator in fluid media is $\omega_{(1)}^{fld} = 52.45\ \text{rad/s}$.

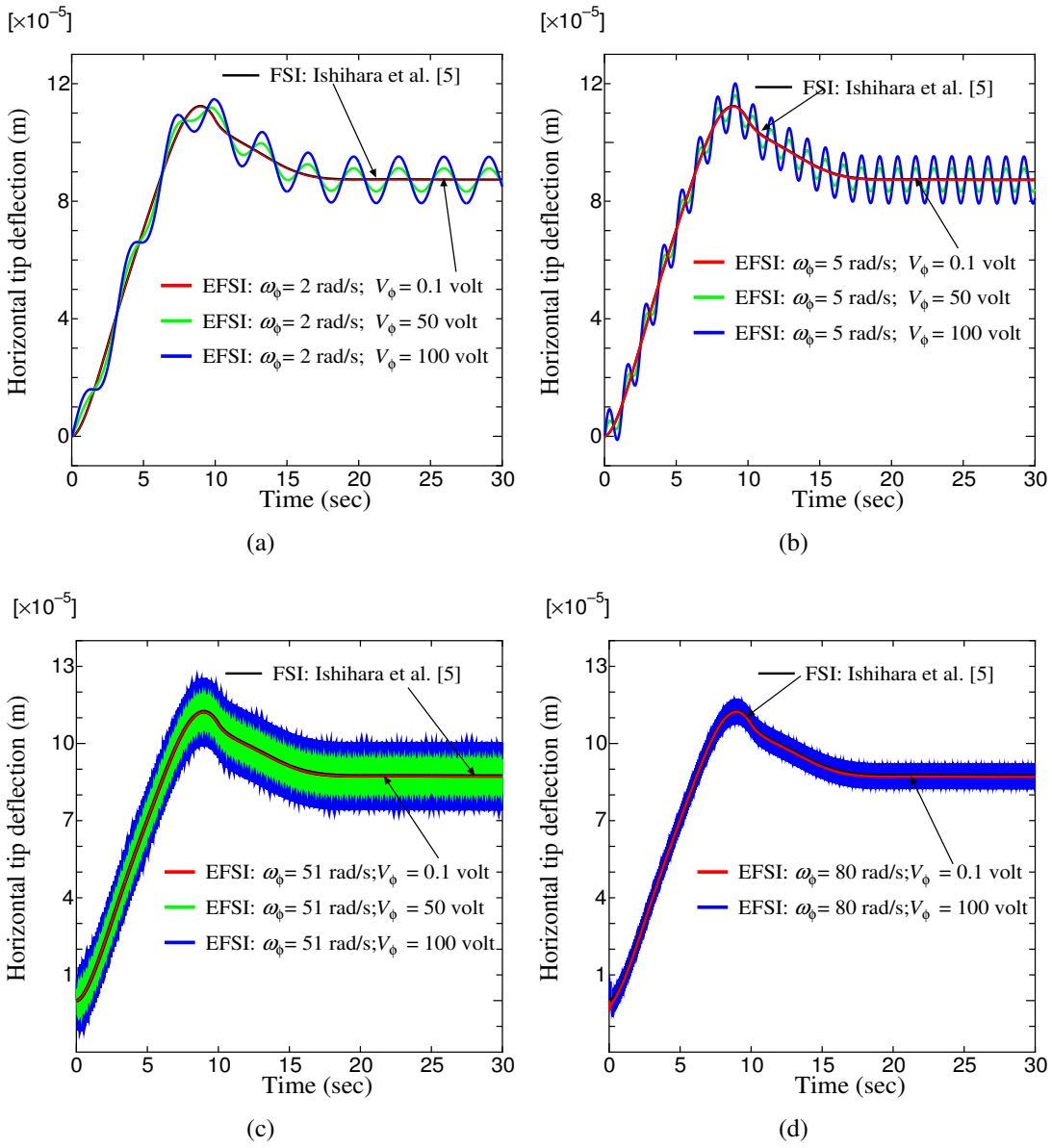

Figure 5: The finite element meshes: (a) Fluid analysis using P1P1 elements, (b)Structure analysis using Shell elements, (c) Electrical analysis using 3D solid elements

Since the FSI benchmark problem has no analytical solution or experimental data, a reference FSI solution obtained using Ishihara and Horie [5] was taken as the exact solution for PVDF material instead of rubber in a silicon oil. Fig. 5 shows the vibration characteristics of the tip of the actuator in response to various input AC signals with different input voltage frequencies. From the theory, the resonance occurs for the input voltage frequency close to the structure resonance. The exact solution for this problem is $\omega_{(1)}^{fld} = 52.45\ \mathrm{rad/s}$. Figs. 5(a), 5(b) and 5(d) show the vibration characteristics for the input voltage frequency far away from the structural resonance in a fluid, while Fig. 5(c) show the response very close to the structure resonance.

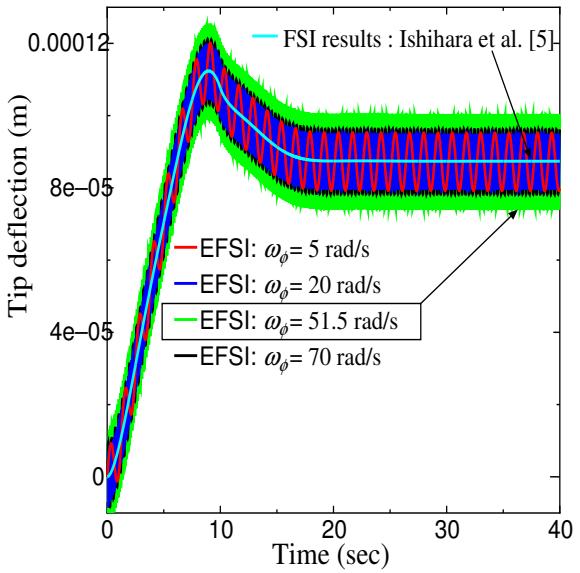

Figure 6: Horizontal displacement of the bimorph actuator at tip at very low input voltage frequency and low bias voltage

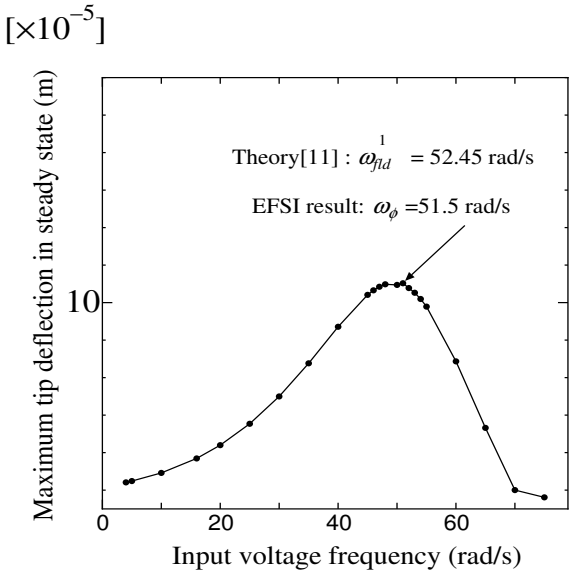

Figure 7: Frequency response curve

One can see in the Fig. 5 that, the response for input voltage $V_{\phi_0} = 0.1\text{volt}$ with frequencies $\omega_\phi = 2, 5, 51 \text{ and } 80 \text{ rad/s}$, the curve coincides with that of the reference solution [5]. This is because the electric forces induced by the inverse piezoelectric effect in the solid elements acting on the shell elements as an externally applied force is very close that of the applied fluid forces on to shell structure in Ishihara and Horie [5]. This indicates that the coupling between electric and fluid–structure interaction is very similar to the fluid–structure interaction. The shape of the present EFSI curve at $V_{\phi_0} = 0.1\text{volt}$ is identical to those from the numerical solutions of Neumann *et al.*[2] and Ishihara and Horie [5]. As the input voltage is increased, the coupling between the electric and fluid–structure interaction becomes significantly strong and harmonic oscillations occurs around the quasi-state phase of the reference solution, as shown in Fig. 5 for $V_{\phi_0} = 50 \text{ and} 100 \text{ volt}$.

Fig. 6 shows the frequency response of the bimorph actuator in a converging channel for the imposed fluid velocity boundary conditions and at a bias voltage $V_{\phi_0} = 100\text{volts}$ for various input voltage frequency ω_ϕ . From the Fig. 6 it is evident that the harmonic oscillations for $\omega_\phi = 5 \text{ rad/s}, 20 \text{ rad/s}, 51.5 \text{ rad/s}, 70 \text{ rad/s}$ are about the reference FSI solution. Fig. 7 shows the maximum horizontal tip displacement obtained using EFSI analysis in the steady state between $t = 25\ 30\ s$ verses input voltage frequency.

Fig. 7 is the summary of the maximum horizontal tip displacement after the time $t = 25\text{s}$ with the input signals with the different frequencies ω_ϕ. It reveals that the EFSI simulation results yielded a maximum displacement at an input voltage frequency $\omega_\phi = 51.5\text{rad/s}$. The relative error between theory and the numerical solution is 1.8%, shows a good agreement.

Next, the equivalent external force F_{ext_0} corresponding to the induced electric forces in a static piezoelectric bimorph actuator problem is applied dynamically as $F_{\text{ext}} = F_{\text{ext}_0} \sin\omega t$ at

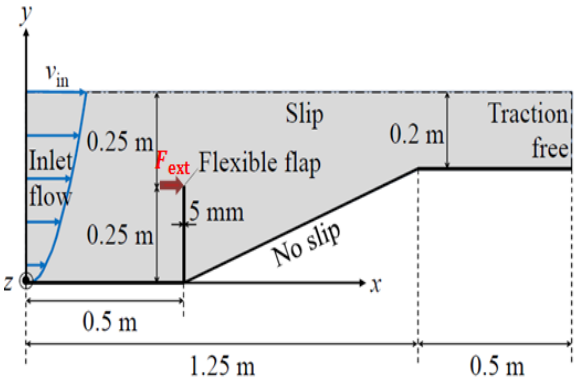

Figure 8: FSI becnhmark problem with dynamic equivalent external mechanical force F_{ext} applied at the tip of the flap

.

the tip of the structure to perform the fluid–structure interaction analysis with the imposed fluid velocity boundary conditions as shown in Fig. 8 using the analysis program of Ishihara and Horie [5]. The purpose of this study is to validate the EFSI solution with that of the reference FSI solution. An external equivalent force corresponding to the induced electric forces in piezoelectric bimorph actuator can be obtained by beam theory,[12]

$$F_{\text{ext}_0} = \frac{3E^s I\delta}{L^3}, \tag{21}$$

where δ is the static tip deflection due to piezoelectric effect in a piezoelectric bimoprh actuator given by [12]

$$\delta = \frac{3L^2}{2t} d_{31} E_3, \tag{22}$$

where d_{31} is the piezoelectric strain constant and $E_3 = V_{\phi_0}/t$ is the applied electric field in the thickness direction (3) of the piezoelectric actuator connected in series type. For an applied input static voltage of $V_{\phi_0} = 100$ volts to a piezoelectric bimorph actuator, the estimated static tip deflection is $\delta = 8.625 \times 10^{-6}$m. The external equivalent forces corresponding to the evaluated static tip deflection is $F_{\text{ext}_0} = 3.45 \times 10^{-4}$N. This static external force F_{ext_0} is applied dynamically as $F_{\text{ext}} = F_{\text{ext}_0} \sin\omega t$ at the tip of the structure as shown in Fig. 8. Here ω is the input frequency of the external equivalent forces.

Fig. 9 shows the frequency response analyzed using FSI algorithm [5] with an equivalent external force applied dynamically at the tip of the actuator is compared with the present EFSI algorithm for bias voltage $V_{\phi_0} = 100$volt. Both the method shows the resonance at frequency 51.5 rad/s. The horizontal displacement of tip computed with the present EFSI approach is close to the FSI solution with equivalent external force at tip until $\omega_{\phi_0} = 40\text{rad/s}$ (Fig. 9). Then it is underestimating slightly because of resonance phenomena as-well as the piezoelectric effect in EFSI approach. But the resonance frequency obtained with both FSI and EFSI match very well and are very close to the theory.

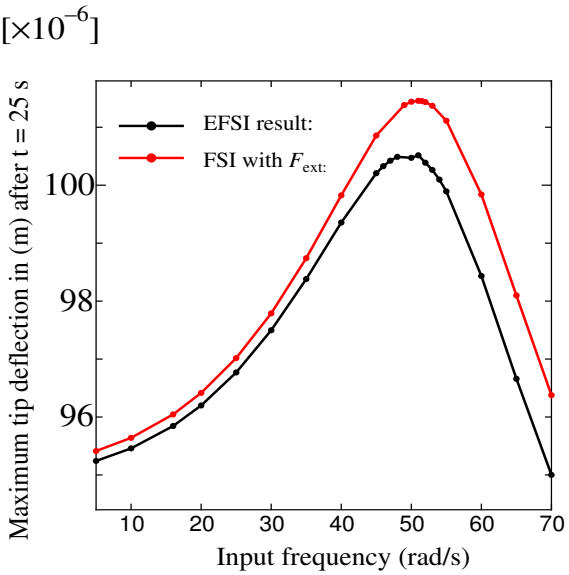

Figure 9: Frequency response curve analyzed using FSI algorithm with equivalent external force and EFSI algorithm

.

4 Conclusions

In this study, a triple coupled algorithm is proposed to analyze electric and fluid–structure–interaction in MEMS applications. The proposed electric and fluid–structure–interaction method takes into account the triple coupled phenomena. The method is the combination of structure–electric interaction and fluid–structure interaction. The horizontal displacement at the tip of the bimorph actuator in converging channel is compared with the reference solution and it shows a good agreement when operated at very low input bias voltage as a fundamental validation. The resonance frequency of the actuator in fluid analyzed using the proposed method well matched with the theoretical solution.

REFERENCES

[1] Ishihara, D. Ohira, N. Takagi, M. and Horie, T. Fluid-Structure Interaction design of insect-like micro flapping wing. *Proc of the VII Int Conf on Computational Methods for Coupled Problems In Science and Engineering (Coupled Problems 2017)*. 870-875.

[2] Neumann, M. Tiyaagura, S.R. and Wall, W.A. Robustness and efficiency aspects for computational fluid–structure–interaction *Computational Science and High Performance Computing II*. (2006) **91**: 99–114.

[3] Prakasha, C.R. Ishihara, D. Niho, T. and Horie, T. Performance evaluation of numerical finite element coupled algorithms for structure-electric interaction analysis of MEMS piezoelectric actuator. *Int J Comput Methods*. (2018) **15**(3): 1850106,28 pages.

[4] Prakasha, C.R. Ishihara, D. Niho, T. and Horie, T. A finite element approach for a coupled numerical simulation of fluid -structure-electric interaction in MEMS.*Proc of the VII Int Conf Computational Methods for Coupled Problems In Science and Engineering (Coupled Problems 2017)*. 999–1007.

[5] Ishihara,D. and Horie,T. A projection method for the monolithic interaction system of an incompressible fluid and a structure using a new algebraic splitting. *CMES-Comp Model Eng*. (2014) **101**: 421–440.

[6] Ishihara,D. and Yoshimura,S. A monolithic approach for interaction of incompressible viscous fluid and an elastic body based on fluid pressure Poisson equation. *Int. J. Numer. Meth. Engng*. (2005) **64**: 167–203.

[7] Zhang,Q. and Hisada, T. Line search partitioned approach for the fluid–structure interaction analysis of flapping wing. *Comput Meth Appl Mech and Engng*. (2001) **190**: 6341–6357.

[8] Tedzuyar, T.E. Mittal,S. Ray, S.E. Shih, R. Incompressible flow computations with stabilized bilinear and linear equal–order–interpolation velocity–pressure elements. *Comput Meth Appl Mech and Engng*. (1992) **95**: 221–242.

[9] Noguchi, H. and Hisada, T. Sensitivity analysis in post buckling problems of shell structures.*Comput Struct*.(1993) **47**:699 – 710.

[10] Felippa, C.A. Park, K.C. and Farhat, C. Partitioned analysis of coupled mechanical systems.*Comput Meth Appl Mech and Engng*.(2001) **190**: 3247–3270.

[11] Van Eysden, C.A. and Sader, J.E. Resonance frequencies of a cantilever beamimmersed in a fluid. *J. Appl. Phys*. (2006) **100**: 114916.

[12] Wang, Q.M. and Cross, L.E. Performance analysis of piezoelectric cantilever bending actuators *Ferroelectrics*.(1998) **215**: 187–213.